

A three-dimensional variational data assimilation system for a size-resolved aerosol model: Implementation and application for particulate matter and gaseous pollutant forecasts across China

Daichun WANG^{1,2}, Wei YOU^{1*}, Zengliang ZANG¹, Xiaobin PAN¹, Hongrang HE¹ & Yanfei LIANG³

¹ Institute of Meteorology and Oceanography, National University of Defense Technology, Nanjing 211101, China;

² No. 94595 Unit of PLA, Weifang 216500, China;

³ No. 32145 Unit of PLA, Xinxiang 453000, China

Received August 19, 2019; revised February 11, 2020; accepted March 19, 2020; published online April 26, 2020

Abstract A three-dimensional variational (3DVAR) data assimilation (DA) system is presented here based on a size-resolved sectional aerosol model, the Model for Simulating Aerosol Interactions and Chemistry (MOSAIC) within the Weather Research and Forecasting model coupled to Chemistry (WRF-Chem) model. The use of this approach means that both gaseous pollutants such as SO₂, NO₂, CO, and O₃ as well as particulate matter (PM_{2.5}, PM₁₀) observational data can be assimilated simultaneously. Two one-month parallel simulation experiments were conducted, one with the assimilation of surface hourly concentration observations of the above six pollutants released by the China National Environmental Monitoring Centre (CNEMC) and one without assimilation in order to verify the impact of assimilation on initial chemical fields and subsequent forecasts. Results show that, in the first place, use of the DA system can provide a more accurate model initial field. The root-mean-square error of PM_{2.5}, PM₁₀, SO₂, NO₂, CO, and O₃ mass concentrations in analysis field fell by 29.27 μg m⁻³ (53.5%), 34.5 μg m⁻³ (50.9%), 30.36 μg m⁻³ (64.2%), 8.91 μg m⁻³ (39.5%), 0.46 mg m⁻³ (47.4%), and 15.11 μg m⁻³ (51.0%), respectively, compared to a background field without assimilation. At the same time, mean fraction error was reduced by 42.6%, 53.1%, 45.2%, 43.1%, 69.9%, and 48.8%, respectively, while the correlation coefficient increased by 0.51, 0.55, 0.48, 0.38, 0.47, 0.65, respectively. Secondly, the results of this analysis reveal variable benefits from assimilation on different pollutants. DA significantly improves PM_{2.5}, PM₁₀, and CO forecasts leading to positive effects that last more than 48 h. The positive effects of DA on SO₂ and O₃ forecasts last up to 8 h but that remains relatively poor for NO₂ forecasts. Thirdly, the influence of assimilation varies in different areas. It is possible that the positive effects of DA on PM_{2.5} and PM₁₀ forecasts can last more than 48 h across most regions of China. Indeed, DA significantly improves SO₂ forecasts within 48 h over north China, and much longer CO assimilation benefits (48 h) are found in most regions apart from north and east China and across the Sichuan Basin. DA is able to improve O₃ forecasts within 48 h across China with the exception of southwest and northwest regions and the O₃ DA benefits in southern China are more evident, while from a spatial distribution perspective, NO₂ DA benefits remain relatively poor.

Keywords WRF-Chem, Aerosol, Gaseous pollutant, 3DVAR, Data assimilation

Citation: Wang D, You W, Zang Z, Pan X, He H, Liang Y. 2020. A three-dimensional variational data assimilation system for a size-resolved aerosol model: Implementation and application for particulate matter and gaseous pollutant forecasts across China. *Science China Earth Sciences*, 63: 1366–1380, <https://doi.org/10.1007/s11430-019-9601-4>

* Corresponding author (email: ywlx_1987@163.com)

1. Introduction

Air pollution influences the work, life, and health of people and has a serious adverse impact on the economic development of society. Due to rapid industrialization and urbanization across China, increasing pollutant emissions and incidents have occurred in recent years. Indeed, regional particulate pollution in China has become an important social and scientific research topic both domestically and in the international literature (Zhang et al., 2014; Zhao et al., 2015; Gao et al., 2015). A nationwide ambient air quality monitoring network comprising more than 1500 stations was established in China in 2013; this network publicly releases hourly mass concentrations as well as 24 h real-time averages for PM_{2.5}, PM₁₀, SO₂, NO₂, CO, and O₃ as well as other pollutants including the air quality index (AQI). These outputs provide important data support for the monitoring, forecast, and control of atmospheric pollutants.

An air quality model (or atmospheric chemistry model) is also a useful tool that can be applied to study atmospheric pollution. These models have been widely utilized in this research field (Binkowski and Roselle, 2003; Xue et al., 2013). Although these approaches play increasingly important roles in the analysis and prediction of aerosol pollution because of rapid technological progress, uncertainties nevertheless remain due to initial chemistry, emission inventories, and mechanisms and adversely affect the prediction. Data assimilation (DA) technology can be used to correct background fields based on observations and to develop a theoretically optimal initial field (Bouttier and Courtier, 2002) and improve forecasting accuracy. Thus, DA has been extensively applied in meteorological operational centers around the world, but research and applications of DA in atmospheric chemistry models were initiated relatively late. The bulk of early research on chemical data assimilation focused on gaseous pollutant compositions and used off-line air quality models to assimilate mass concentrations of O₃, NO_x, SO₂, CO and other gases based on air quality models (Elbern et al., 1997; Eibern and Schmidt, 1999; Elbern and Schmidt, 2001; Errera et al., 2008). Particulate matter PM_{2.5} and PM₁₀ observations were therefore assimilated. The control variables in early assimilation systems applying aerosol data were therefore total mass concentration of PM_{2.5} or PM₁₀ because of computational cost and observational data limitations. These studies were unable to consider interactions between multiple chemical species and particle sizes. Assimilation methods are also relatively simple, for example the Optimal Interpolation (OI) approach. In one early study, Cui et al. (2006) used OI to assimilate total mass concentration of PM₁₀ based on nested grid air quality model, and the results showed that DA significantly reduces model prediction bias and root mean square errors. Tombette et al. (2009) applied OI to assess the assimilation

of total PM₁₀ mass concentrations across Europe and was able to show that the use of DA significantly improves forecasting accuracy. Similarly, Niu et al. (2007) constructed a 3DVAR assimilation system as a sandstorm forecast model for China incorporating the total mass concentration of dust aerosols with diameters less than 40 μm as the control variable.

In light of the development of online coupled meteorology-aerosol models (Grell et al., 2005), as well as enhanced research on the mutual feedback between aerosols and weather, DA aimed at coupled meteorology-aerosol models has also gradually developed. The assimilation method in this context mainly applies sequential and variational approaches as more-and-more observations from various platforms become available and are added to the model (Lin et al., 2008; Pagowski and Grell, 2012). In one example, Jin et al. (2016) assimilated mass concentrations of PM_{2.5} and PM₁₀ using the 3DVAR method based on the WRF-Chem model, and the results showed that assimilation significantly improved the initial field and its positive effect could last up to 20 h. Pagowski et al. (2010) applied 3DVAR within a Grid-point Statistical Interpolation (GSI) system to assimilate surface PM_{2.5} and O₃ mass concentrations over North America using the WRF-Chem model. The results of this analysis indicated that improved PM_{2.5} and O₃ forecasts via DA can last for at least 24 h (Pagowski et al., 2010). Progress has also been made in terms of computing speed and developments in DA technology including the incorporation of aerosol chemical components as control variables in many studies and reductions in the use of intermediate conversion steps. In one example, Jiang et al. (2013) performed a PM₁₀ mass concentration assimilation experiment using GSI applying the Goddard Global Ozone Chemistry Aerosol Radiation and Transport model (GOCART) aerosol scheme again in the WRF-Chem model. Aerosol variables in GOCART were thus used directly as control variables in the assimilation system. The results of this analysis revealed that DA can effectively improve PM₁₀ forecasts for up to 12 h (Jiang et al., 2013). In another approach, Li et al. (2013) considered PM_{2.5} on the basis of five chemical species using the MOSAIC aerosol scheme (Zaveri et al., 2008) again in the WRF-Chem model and independently constructed a 3DVAR assimilation system in which surface PM_{2.5} concentrations were assimilated to perform a simulation experiment. The results of this analysis also showed that DA has a beneficial effect on both the initial field and PM_{2.5} forecasts within a 24 h period (Li et al., 2013). Subsequently, Cheng et al. (2019) developed the Community Radiative Transfer Model (CRTM) based on the MOSAIC scheme in WRF-Chem to enable lidar extinction coefficients to be assimilated using the 3DVAR method. The results of this analysis revealed that DA can significantly enhance PM_{2.5} simulations of surface concentrations and vertical structures.

In earlier work, Schwartz et al. (2012) had used GSI to assimilate PM_{2.5} mass concentrations and satellite Aerosol Optical Depth (AOD). These results showed that simultaneous assimilation of aerosol data from various observation platforms can be applied to synergistically improve aerosol forecasts. Numerous scholars have subsequently performed assimilation experiments using satellite AOD and surface routine observational data applying different air quality models within a GSI assimilation system framework (Saide et al., 2014; Tang et al., 2017; Feng et al., 2018).

The studies discussed here all suggest that optimizing a model initial field using DA technology can significantly improve aerosol forecasts. The bulk of assimilation studies so far associated with WRF-chem, however, have been based on the relatively simple GOCART scheme developed for a GSI assimilation system. As this system mainly describes the chemical mechanisms of dust aerosols, nitrate and ammonium salt components are not included alongside corresponding secondary reaction processes. As we now have a deeper understanding of the chemical mechanisms underlying anthropogenic aerosols as well as richer observational data, the application of MOSAIC multi-species in multi-particle size sections aerosol mechanism to anthropogenic sources in China has become more and more attractive (Chen et al., 2016). Aerosol particles and gaseous pollutants have also generally been assimilated separately in previous studies; few workers have considered the simultaneous assimilation of aerosol particles alongside gaseous pollutant observations. A 3DVAR assimilation framework is presented in this study that was developed based on the MOSAIC scheme to distinguish the reaction characteristics of components at different size sections. This framework was constructed independently using the WRF-Chem model and the control variables that were included comprise eight components of aerosols, particles, and gaseous pollutants. Simulation experiments to assess the simultaneous assimilation of gaseous pollutants (i.e., SO₂, NO₂, CO, and O₃) as well as aerosol particle routine measurements were performed for a month to study the impacts of assimilation on different pollutant forecasts and to provide a reference for pollutant forecasts, analysis, and related research.

2. The model and DA algorithm

2.1 Model configuration

The WRF-Chem model is a regional atmospheric chemistry model that was constructed coupled to the WRF model. As an online-coupled numerical model (Grell et al., 2005), WRF-Chem can incorporate feedback from chemical substances in meteorological fields and simulate weather elements and atmospheric chemical compositions simultaneously. The model also includes a variety of atmo-

spheric chemistry parameterization schemes and can effectively simulate a range of processes including pollutant transport, deposition, gas-phase mechanisms, emissions, aerosol parameterization, and photolysis. This approach has therefore been widely applied in atmospheric pollutant analysis and forecasting (Han et al., 2008; Chen et al., 2016; Song et al., 2017). The main physical and chemical parameterization schemes used in this paper are listed in Table 1. It is noteworthy that the MOSAIC 4bins aerosol scheme is preferable (Zaveri et al., 2008) in this context because it incorporates tradeoffs between aerosol detailed descriptions, including chemical components, particle size distributions, and computational cost. This scheme is therefore popular amongst researchers. The MOSAIC scheme divides atmospheric aerosols into eight components, carbon black (BC), organic carbon (OC), nitrate (NO₃), sulfate (SO₄), chloride (Cl), sodium (Na), ammonium salts (NH₄), and inorganics (OIN). Thus, four particle size bins are utilized for individual components, between 0.039 μm and 0.1 μm, between 0.1 μm and 1.0 μm, between 1.0 μm and 2.5 μm, and between 2.5 μm and 10 μm, respectively. The sum of the components in the first three sections corresponds to PM_{2.5}, while the fourth corresponds to PM_{2.5–10} (i.e., PM₁₀ minus PM_{2.5}). A total of 32 model variables are therefore used to describe aerosols in the MOSAIC scheme. Here, WRF-Chem version 3.7 was used for simulation experiments; the simulation domain was centered at (101.5°E, 37.5°N), grids were not nested and were set at a 27 km horizontal grid spacing to cover most parts of East Asia (Figure 1). The model therefore includes 210 grid points in an east-west direction and 168 grid points in a north-south direction with 40 vertical model layers.

2.2 3DVAR algorithm

The 3DVAR assimilation method merges background field information and observations organically to create a model analysis field with minimum error variance based on the idea of optimal estimation (Bouttier and Courtier, 2002). The objective function of 3DVAR assimilation is as follows:

$$J(x) = \frac{1}{2}(x - x_b)^T B^{-1}(x - x_b) + \frac{1}{2}(Hx - y)^T R^{-1}(Hx - y). \quad (1)$$

In this expression, x is a vector of analysis field that defines control variables in the assimilation system, x_b is the background state vector, y is the observation vector, B is the background error covariance matrix which encompasses forecasting errors, and R is the observation error covariance matrix associated with observational errors. It is thought that R is a diagonal matrix; thus, building on the earlier work of Li et al. (2013), observational errors were set to half the background error standard deviations (SDs) of each control variable. H is an observation operator that transforms the model variables into this space. As a linear operator, H

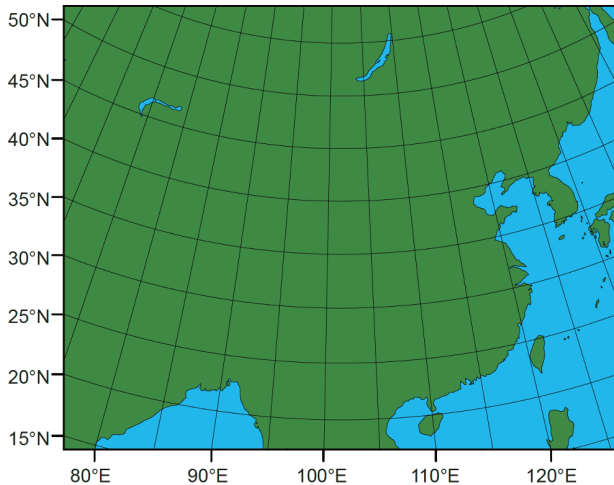


Figure 1 Map to show the simulation domain.

Table 1 Model parameterization schemes

Physical or chemical process	Option
Cloud microphysics	WSM 5-class
Longwave radiation	RRTMG
Shortwave radiation	RRTMG
Land surface	Noah
Planetary boundary layer	YSU
Cumulus convection	New Grell
Aerosol	MOSAIC 4 bins
Anthropogenic source	RADM2/MADE/SORGAM
Photolysis	Fast-J

mainly performs interpolations of simulated values from grid points to observational locations. The 3DVAR DA mathematically searches for a solution to minimize this objective function; as this is usually a problem involving significant dimensions, numerical optimization algorithms are applied. The minimum solution obtained is therefore considered statistically optimal.

The design of control variables in the assimilation system is also important. It is generally the case that the more control variables are included, the more accurate the analysis field. It is, however, unrealistic to regard all model variables of a three-dimensional grid that accurately describe aerosol as control variables because of the limits of computational speed and storage capacity. This means that control variables should provide an optimal combination of model aerosol variables. We therefore designed control variables for this analysis according to available observational data. Two control variables were designed for each of the eight components in the MOSAIC scheme; one of these is the sum of model variables from the first three size sections, denoted respectively as EC_i, OC_i, CL_i, NA_i, NH4_i, NO3_i, SO4_i, and OIN_i (see below) which correspond to the PM_{2.5} component.

The second is the variable from the fourth size section, denoted as EC_j, OC_j, CL_j, NA_j, NH4_j, NO3_j, SO4_j, and OIN_j (see below) which correspond to the remainder of PM₁₀ minus PM_{2.5}. The number of control variables used to assimilate particulate matter observations decreases from 32 to 16 and also causes a significant reduction in computation cost. Four gaseous model variables (i.e., SO₂, NO₂, CO, and O₃) can also be directly assimilated leaving 20 control variables in the assimilation system. Particulate matter (PM_{2.5} and PM₁₀) and gaseous pollutant (i.e., SO₂, NO₂, CO, and O₃) measurements can be assimilated simultaneously in this system.

3. Background error covariance

One core issue in DA is estimating background error covariance (BEC). This is important because it not only restricts the spread of corrections caused by observation information in model space but also determines the relative weight of observational and background information across the analysis field (Derber and Bouttier, 1999). Thus, once control variables are designed, it is necessary to calculate the BEC of each control variable. The NMC method (Parrish and Derber, 1992) has been used regularly to calculate BEC values for traditional meteorological fields such as temperature and wind and is also appropriate for aerosol component mass concentrations (Benedetti and Fisher, 2007; Liu et al., 2011; Li et al., 2013). The NMC method was used here to compute background error SD and the attenuation scale of horizontal correlation coefficients for each control variable. This enabled BECs to be determined via parameter estimation. The NMC method utilizes the differences between 48 h and 24 h forecasts valid at the same time (0000 UTC) between October 11th 2017 and November 10th 2017 to approximately estimate BECs.

The computation of matrix B is generally very intensive when a high-resolution numerical model is used; this means that it is very costly and difficult to store and find an inverse and so certain mathematical preprocessing steps are necessary. The same methods were therefore used here to compute B as outlined in Li et al. (2013). Thus, in the first step, B can be represented as the product of matrices, $B = D C D^\top$, where D is the background error SD matrix and C is the background error correlation matrix. As we assume that the background errors of different variables are not correlated, C becomes a blocked diagonal matrix. This means that C can be further expressed as $C = C_x U C_y U C_z$, where U denotes Kronecker product, also known as the vector or tensor product. Thus, C_x , C_y , and C_z denote correlation submatrices in the longitude, latitude, and vertical coordinate directions, respectively. We also assume that C_x and C_y are isotropic horizontally and identical vertically such that can be fitted

using a one-dimensional Gaussian function. The C_x between two arbitrary points x_1 and x_2 can therefore be expressed as follows:

$$C_x = e^{[-(x_1 - x_2)^2 / 2(L_x)^2]}. \quad (2)$$

In this expression, L_x denotes the attenuation scale of horizontal correlation. This determines the horizontal correlation and can be calculated via model output; thus, as the correlation between two points generally decreases as distance increases, L_x is defined as the distance at which the correlation decreases to $e^{-1/2}$. Vertical correlation, C_z , is more important for the analysis of pollutant vertical transport and is estimated directly from the model background field using the NMC method.

The vertical distribution of mass concentration background error SDs for every control variable is shown in Figure 2. These SDs differ among chemical components and exhibit a common decrease with height apart from O_3 (Figure 2). The most rapid decrease is seen between 1000 and 2000 m (i.e., between level 20 and level 25). Diminishing rates also vary amongst chemical components with the largest seen in OINj. It is also the case that the background error SD of O_3 starts to increase with height, reaching a peak between 280 and 490 m before decreasing again into the upper troposphere. There also appears to be another peak in the stratosphere (Figure 2). The vertical profile of the background error SD corresponds to the vertical concentration distribution of this chemical component. This means that higher concentrations tend to have larger background error SDs. Ground-level concentrations from high-to-low in sequence are OINj, O_3 , NO3i, SO₂, NO₂, OINi, NH4i, SO4i, OCi, and ECi. The concentrations of other chemical components are very low from the ground to the air and all have error SDs below 0.05.

A horizontal correlation of background error determines the propagation of observation information in this direction. This means that correlations among different control variables are not taken into account, just auto-correlations at different distances. An attenuation scale, L_x , for individual control variables is presented in Table 2 and differs amongst chemical components. Thus, out of all chemical components, SO4i reaches a maximum value at 65.1 km; this suggests that the influence of SO4i extends further than other components and has a larger-domain improvement across the background field. In contrast, CLj reaches a minimum value of 16.5 km and spreads the least based on observational information.

The background error vertical correlation determines the vertical diffusion of chemical component concentrations. Statistical auto-correlations for control variables are given in Figure 3. This figure presentation shows that auto-correlations differ among chemical components and that all decrease with height. In terms of aerosol chemical components, data show that SO4i diffuses furthest vertically, consistent

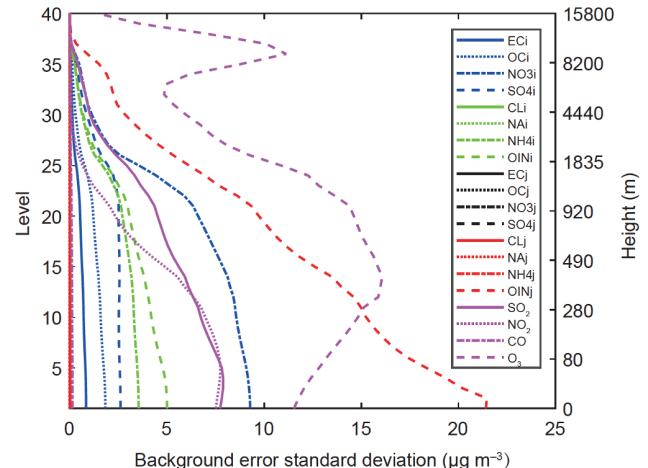


Figure 2 Vertical profile of the background error SD for control variables ECi, OCi, NO3i, SO4i, CLI, NAI, NH4i, OINI, ECj, OCj, NO3j, SO4j, CLj, NAIj, NH4j, and OINj. These are proxies for various aerosol components and were calculated alongside the gaseous pollutants SO_2 , NO_2 , CO, and O_3 .

Table 2 Attenuation scale for background error horizontal correlation coefficients for individual control variables

Control variable	Attenuation scale (km)	Control variable	Attenuation scale (km)
ECi	55.4	ECj	53.8
OCi	55.7	OCj	53.9
NO3i	51.2	NO3j	44.7
SO4i	65.1	SO4j	55.6
CLI	26.1	CLj	16.5
NAi	56.3	NAj	48.6
NH4i	58.4	NH4j	50.1
OINI	53.9	OINj	44.9
SO ₂	47.6	CO	54.4
NO ₂	39.5	O ₃	49.2

with horizontal results, while CLj diffuses least. Chloride (Cl) and sodium (Na) also spread less than their counterparts because of low concentration levels, while in terms of gaseous pollutant, CO spreads furthest while NO_2 spreads least in a vertical plane. All pollutants are confined to the troposphere; more tend to accumulate closer to the ground.

4. Data and methods

On the basis of the assimilation system described above, two comparative experiments were performed as part of this analysis. These were control and assimilation experiments, referred to as Control and Assimilation, respectively. These experiments were both initialized at 0000 UTC each day in order to present 48 h forecasting. The experiments were run from October 11th 2017 to November 10th 2017, both over a period of one month. The same physical and chemistry

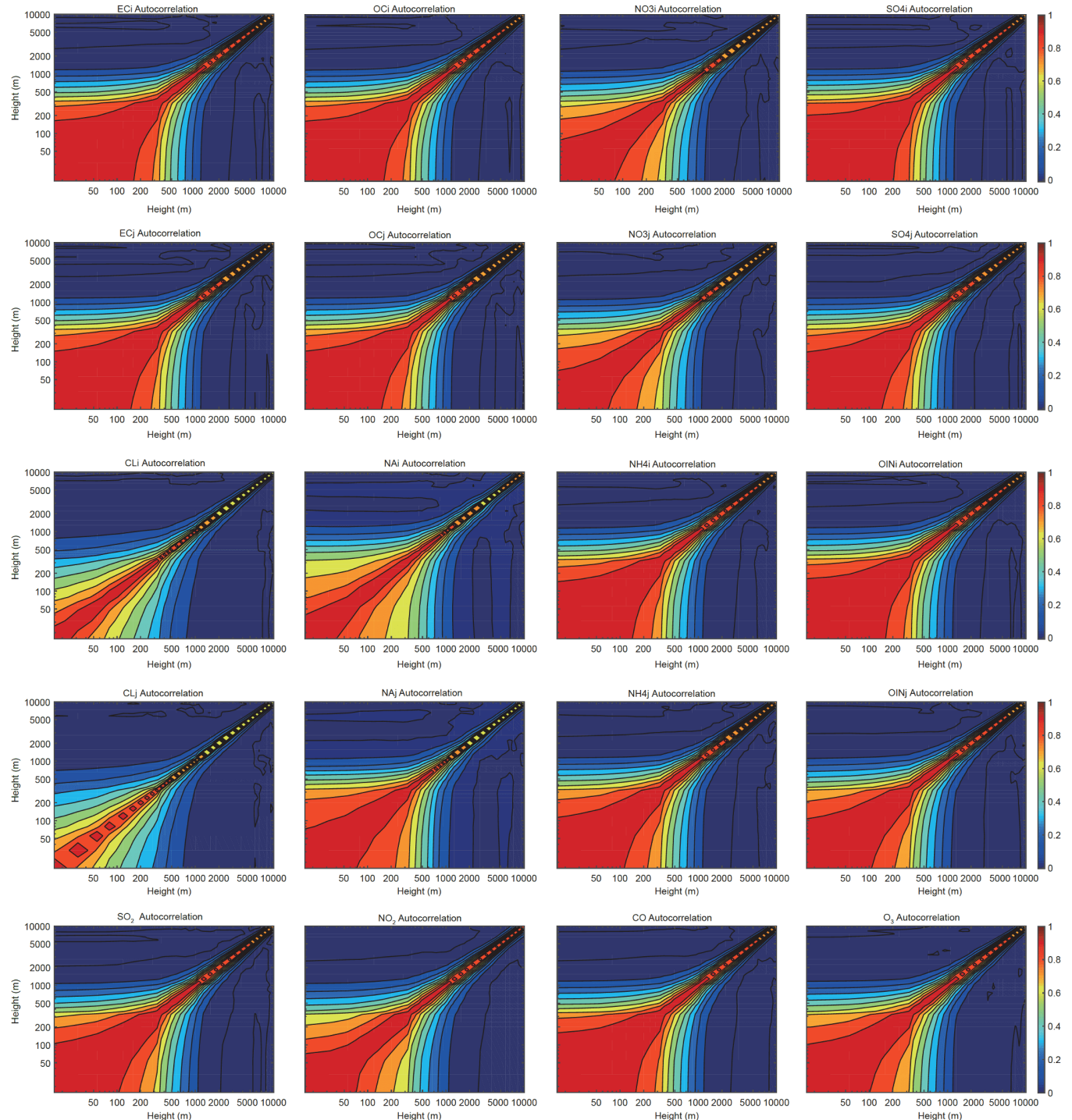


Figure 3 Vertical auto-correlation of background errors for control variables ECi, OCi, NO3i, SO4i, CLi, NAI, NH4i, OINi, ECj, OCj, NO3j, SO4j, CLj, NAj, NH4j, and OINj, all proxies for various aerosol components, as well as the gaseous pollutants SO₂, NO₂, CO, and O₃.

parameterization schemes were used in both experiments, as shown in Table 1. We applied the final (FNL) Operational Global Analysis data over a 6 h interval and using 1-degree by 1-degree resolution as presented by the National Centers for Environmental Prediction (NCEP) in order to generate the initial and lateral boundary conditions of meteorological fields driving the model. The only difference between the two experiments was the initial chemical field. Thus, the

Control experiment assimilated no observations and simply used the previous 24 h forecasts as the initial field for the next run while the Assimilation experiment employed the analysis field as initial conditions after assimilating particulate matter and gaseous pollutant mass concentrations at 0000 UTC. The source emission inventory used was the 2010 Multi-resolution Emission Inventory for China that was collated by Tsinghua University (<http://www.meicmodel>.

[org/index.html](#)), while the observational data used in this study was obtained from the national urban air quality real-time release platform of CNEMC (<http://106.37.208.233:20035/>), which included real-time monitoring data from 1497 stations. Either Figure 6 or Figure 7 shows that the distribution of air quality monitoring sites across the country is dramatically uneven; this distribution is dense in the east but sparse in the west, concentrated mostly in cities while few are located in suburbs and mountainous areas. Quality control of observational data is also necessary before it can be used. The methods applied in this context include extreme value limitation, excluding data greater than 600 for PM_{2.5}, 700 for PM₁₀, 350 for SO₂, 250 for NO₂, 200 for O₃, and 10 for CO, respectively. Units for CO concentration are mg m⁻³ while all other values are presented as µg m⁻³. Another method applied here is abnormal value processing, excluding observational values less than zero as well as those that do not vary over consecutive 24 h periods.

In order to quantitatively evaluate the positive effects of assimilation on model prediction, statistical indicators were utilized. Thus, Correlation Coefficient (CORR), Root Mean Squared Error (RMSE), Mean Fraction Error (MFE) as well as other indicators were introduced in order to evaluate model performance (Boylan and Russell, 2006). The first of these, CORR, reflects the correlation between simulated and observational values, while RMSE, along with MFE, quantifies systematic errors associated with the model. The three indicators were also used to assess DA performance. This means that when comparing between two experiments, interpolated simulated values from regular grid-points to observational locations were initially resolved to generate simulated-observational data pairs at each site. We then computed these indicators for each experiment as either a function of the forecast range (i.e., 48 h), taking pairs from all observation sites as a sample, or as a space function, taking pairs within the forecast range from each site as a sample. Calculated indicators were therefore able to verify the impact of assimilation benefits on forecasting and its duration. These were also able to illustrate the spatial differences in assimilation benefits for one pollutant. In order to eliminate the effect of randomness, indicators were averaged over one month to generate a general result.

5. Results

5.1 Assimilation benefits for initial fields

The purpose of assimilation is to enhance the initial chemical field. This means that the forecasting accuracy of pollutants can be improved by optimizing the initial field. The presentation in Figure 4 depicts simulated mass concentrations

of pollutants in initial fields for both Control and Assimilation experiments versus surface observations. Thus, as shown in Figure 4a (PM_{2.5}), blue dots are scattered on both sides of a central line as partial simulations remain relatively low compared with observations. This means that, for sites where observations more than 300 µg m⁻³ were recorded, corresponding simulations do not exceed by 100 µg m⁻³. Subsequent to assimilation, red dots are more densely distributed on both sides of the line than their blue counterparts. This is especially the case for those with observed values higher than 300 µg m⁻³ and with simulated values less than 100 µg m⁻³; in these cases, DA significantly enlarges simulations so that they are closer to observations. Indeed, in terms of evaluation indicators, CORR values for simulations versus observations increased from 0.34 to 0.85 via DA while RMSE values decreased from 54.67 to 25.40 µg m⁻³, a decrease of 29.27 µg m⁻³ (53.5%). At the same time, MFE values decreased from 0.68 to 0.39, a reduction of 0.29 (42.6%). The data in Figure 4b summarizing PM₁₀ are similar to PM_{2.5}; in this case, the analysis field after assimilation is closer to observations than the background field. Statistical indicators show that CORR increased from 0.29 to 0.84, while RMSE decreased from 67.76 to 33.26 µg m⁻³, a decrease of 34.50 µg m⁻³ (50.9%). At the same time, MFE values decreased from 0.64 to 0.30, a decrease of 0.34 (53.1%). It is also noteworthy that the RMSE of PM₁₀ underwent a large decrease because it includes the reduction in PM_{2.5}. As presented in Figure 4c (SO₂), blue dots are distributed across a triangular field with most stacked parallel with the vertical axis; this indicates that simulated concentrations of SO₂ in the background field are high, which may be related to the active chemical properties of SO₂ as well as the parameterization schemes applied in this analysis. Subsequent to assimilation, red dots are situated on both sides of the line; although not very dense, the shape and direction of this distribution is consistent with the central line. Results also show that CORR values increased from 0.12 to 0.60, while RMSE values decreased from 47.31 to 16.95 µg m⁻³, a reduction of 30.36 µg m⁻³ (64.2%). At the same time, MFE values decreased from 0.93 to 0.51, a decrease of 0.42 (45.2%). Data for NO₂ (Figure 4d) show that red dots are distributed more densely than their blue counterparts along the line. Indicators show that CORR values increased from 0.44 to 0.82, while RMSE values decreased from 22.53 to 13.62 µg m⁻³, a reduction of 8.91 µg m⁻³ (39.5%). MFE values also decreased from 0.51 to 0.29, a reduction of 0.22 (43.1%). Data for CO (Figure 4e) show that almost all blue dots are located below the line with a majority far distant; this indicates that simulated concentrations of CO remain significantly low, perhaps attributable to a large underestimation of source emissions. The DA process generally enlarges CO concentrations within the analysis field so that they are much closer to observations, especially for sites

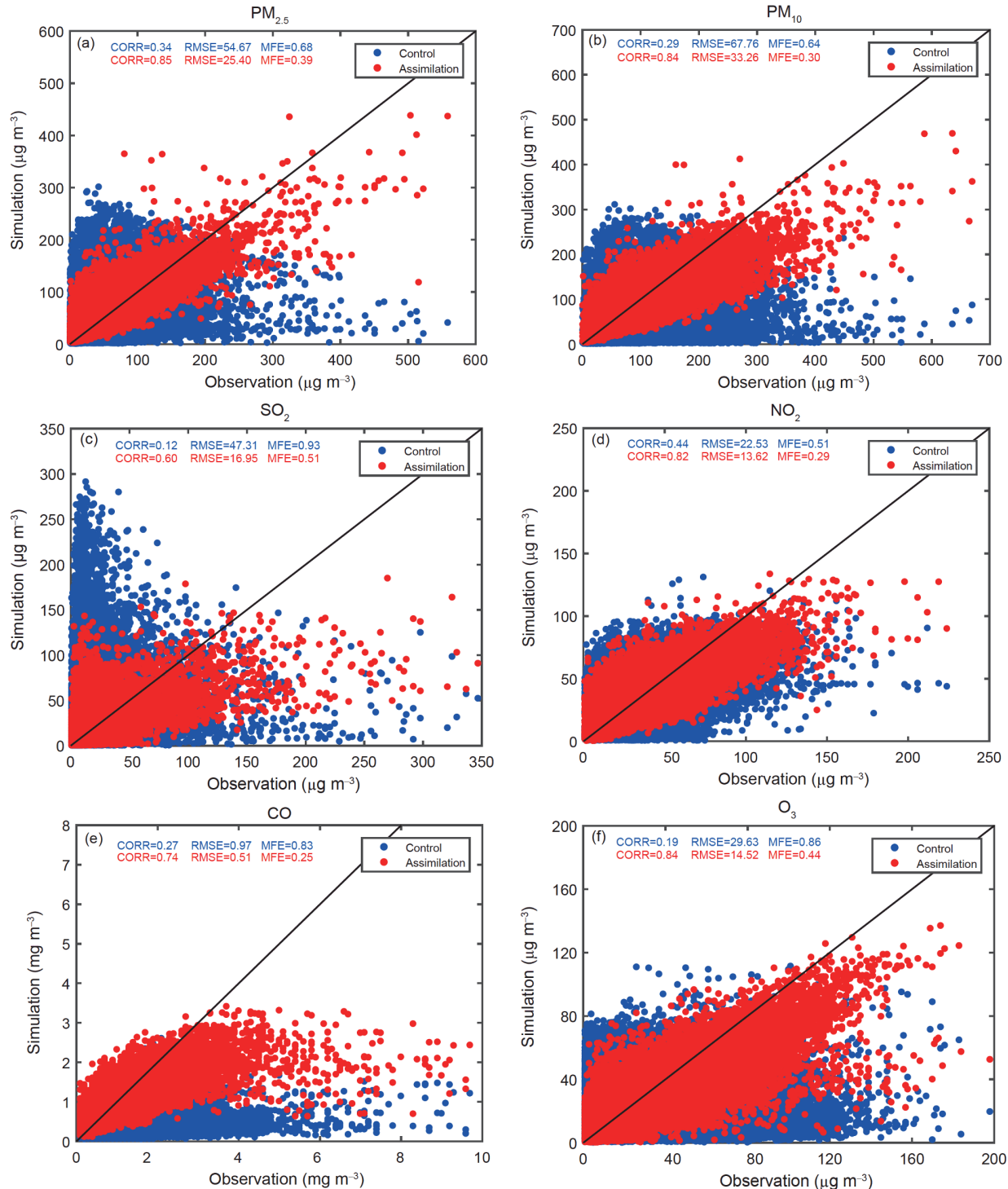


Figure 4 Scatter plots to show simulation-observation data pairs for (a) PM_{2.5}, (b) PM₁₀, (c) SO₂, (d) NO₂, (e) CO, and (f) O₃ mass concentrations at all observation stations. These data were all collected at 0000 UTC over the period October 11th 2017 to November 10th 2017 from Control (blue) and Assimilation experiments (red). The line shows the point at which simulations are equal to observations.

where these are less than 2 mg m⁻³ and thus simulated concentrations are symmetrically located along the line after assimilation. Simulated concentrations for those with large observations (such as more than 3 mg m⁻³) remain significantly low after assimilation indicating that enlargement

is not sufficient in these cases. Statistical indicators show that CORR values increased from 0.27 to 0.74, while RMSE values decreased from 0.97 to 0.51 mg m⁻³, a fall of 0.46 mg m⁻³ (47.4%). Values for MFE also decreased from 0.83 to 0.25, a decrease of 0.58 (69.9%). Data for O₃ (Figure

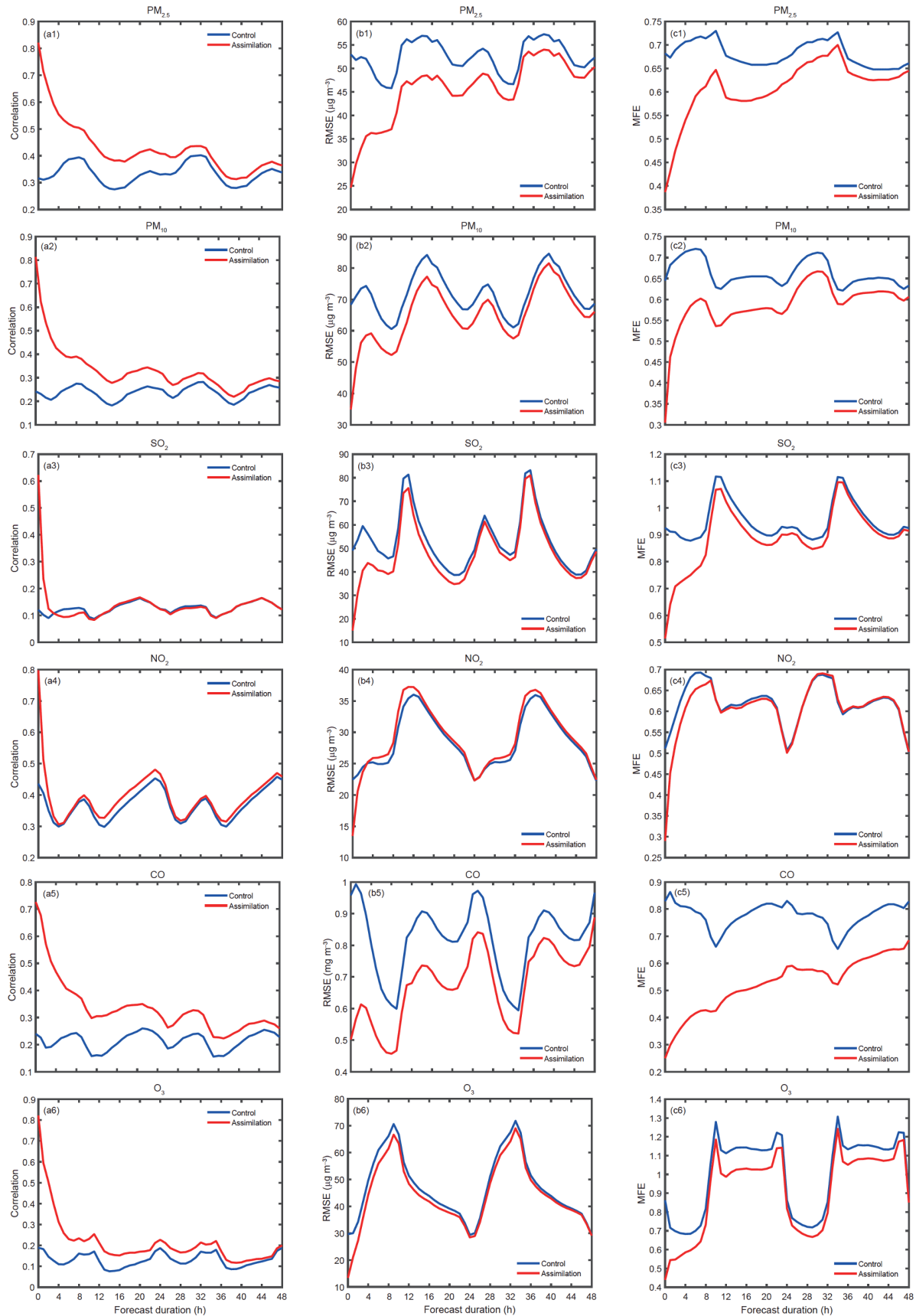


Figure 5 Evaluation indicators (a) CORR, (b) RMSE, and (c) MFE for Control (blue) and Assimilation experiments (red) as a function of forecast range regarding pollutants $\text{PM}_{2.5}$, PM_{10} , SO_2 , NO_2 , CO , and O_3 , respectively, from top-to-bottom.

4f) show that red and blue dots are situated on both sides of the line but that the red ones are more compact and closer to observations than their blue counterparts. Statistical indicators show that CORR values increased from 0.19 to 0.84, while RMSE values decreased from 29.63 to 14.52 $\mu\text{g m}^{-3}$, a decrease of 15.11 $\mu\text{g m}^{-3}$ (51.0%). MFE values also decreased from 0.86 to 0.44, a reduction of 0.42 (48.8%).

5.2 Assimilation benefits for forecasting

Due to model systematic errors, meteorological conditions, and uncertainties in source emissions, the positive effects of DA on pollutant forecast improvements are likely to fade and even disappear as integration time increases. This means that improvements and duration are also different among different pollutants. The data presented in Figure 5 reveals time variation in evaluation indicators for Control and Assimilation experiments within the forecast range for different pollutants. Data show that aerosol ($\text{PM}_{2.5}$ and PM_{10}) simulations in the Assimilation experiment performed better than in the Control experiment, irrespective of CORR, RMSE, or MFE values and that improvement due to DA was sustained for more than 48 h. Differences between indicators in these two experiments were greatest at the initialization point before they decreased gradually in a fluctuating way with integration time. Difference diminished rapidly in the initial hours, when benefits from assimilation decreased rapidly; this might be due to the forcing of emissions in addition to vertical mixing and advection (Jiang et al., 2013). Values also fell slowly after integration over a certain time while the trend of the two indicator curves remains roughly the same. In one example, the benefits of DA for PM_{10} RMSE values diminished rapidly over the first 4 h while those for $\text{PM}_{2.5}$ decreased over the first 8 h. At the same time, the RMSE of PM_{10} is larger than that of $\text{PM}_{2.5}$ and the CORR of PM_{10} is smaller than that of $\text{PM}_{2.5}$; these differences may be due to coarser particle sizes, shorter residence time, and reduced propagation of PM_{10} in the air compared with fine particular matter. Forecast error can also vary with simulated concentrations; as higher simulations tend to have larger forecast errors, the RMSE curve reflects the daily variation characteristics of aerosol concentrations. It is clear that peak $\text{PM}_{2.5}$ concentration mostly occurs at night, with a trough around 16:00 (Shang et al., 2018). Diurnal variation in PM_{10} concentration is also more marked than that of $\text{PM}_{2.5}$; the main peak appears at night, followed by a low level in the morning, and a trough around 16:00 (Ma et al., 2018; Shang et al., 2018). It is noteworthy that these characteristics appear to represent a general case countrywide rather than being specific for a certain place and are closely related to diurnal variations in weather conditions. Radiation cooling at night is enhanced and the inversion layer is not conducive to the upward diffusion of pollutants while a weaker wind at night

is not conducive to the horizontal transport, which led to an accumulation of pollutants. Thermal convection in the afternoon is strong, in contrast, conducive to the diffusion and dilution of pollutants.

The assimilation benefits of gaseous pollutants are summarized in Figure 5. These data show that the positive effect of DA significantly improves the initial field and subsequent forecasts of CO concentration over 48 h. This effect then weakens and fluctuates as forecasting time increases. The CORR of CO simulations versus observations in the initial field obviously increases after observations were introduced into the model. Two troughs then occur in the RMSE time series curve, indicating that the lowest CO concentrations appear at around 16:00 (Ma et al., 2018; Shang et al., 2018). Although assimilation significantly improves the initial field of SO_2 and NO_2 , this improvement is temporary perhaps because these pollutants are unstable and easily participate in chemical reactions. This might also be due to the fact that the chemical parameterization schemes applied in this experiment were not accurate enough. In terms of both RMSE and MFE, improvements in SO_2 forecasts due to DA can last for 8 h and show negligible improvements afterwards. In terms of CORR values, improvements decrease rapidly after the first two hours while SO_2 CORR values remain relatively small compared with other pollutants, something which might be related to the model. The RMSE curve reflects the fact that peak SO_2 concentration usually occurs at night and a trough is seen at 0400 and 1500. In terms of statistical indicators, both CORR and RMSE values reflect the fact that improvements in NO_2 forecasts due to DA are weaker; just the initial field and forecasts within the first 3 h benefit from DA which indicates that NO_2 forecasts are more seriously affected by factors other than assimilation. MFE values show that the positive effects of DA appear to continue for around 9 h. The RMSE curve generated here shows that the peak of NO_2 concentration appears at night. Subsequent to DA, O_3 CORR improves significantly and the improvement is maintained for about 44 h. It is clear that both RMSE and MFE values reflect the fact that improvements diminish rapidly after the first 3 h and are maintained for about 8 h before becoming negligible subsequently. The RMSE time series curve generated here indicates that the peak of surface O_3 concentration appears at about 1700 (Shang et al., 2018).

5.3 Spatial assimilation benefits

The benefits of DA can vary spatially due to different pollution levels, emissions, and meteorological conditions in each region. This means that a comparison of evaluation indicators between the two experiments can be used to analyze the spatial distribution of benefits. The data presented in Figure 6 summarize evaluation indicators for different pollutants averaged over 31 simulations in the Control

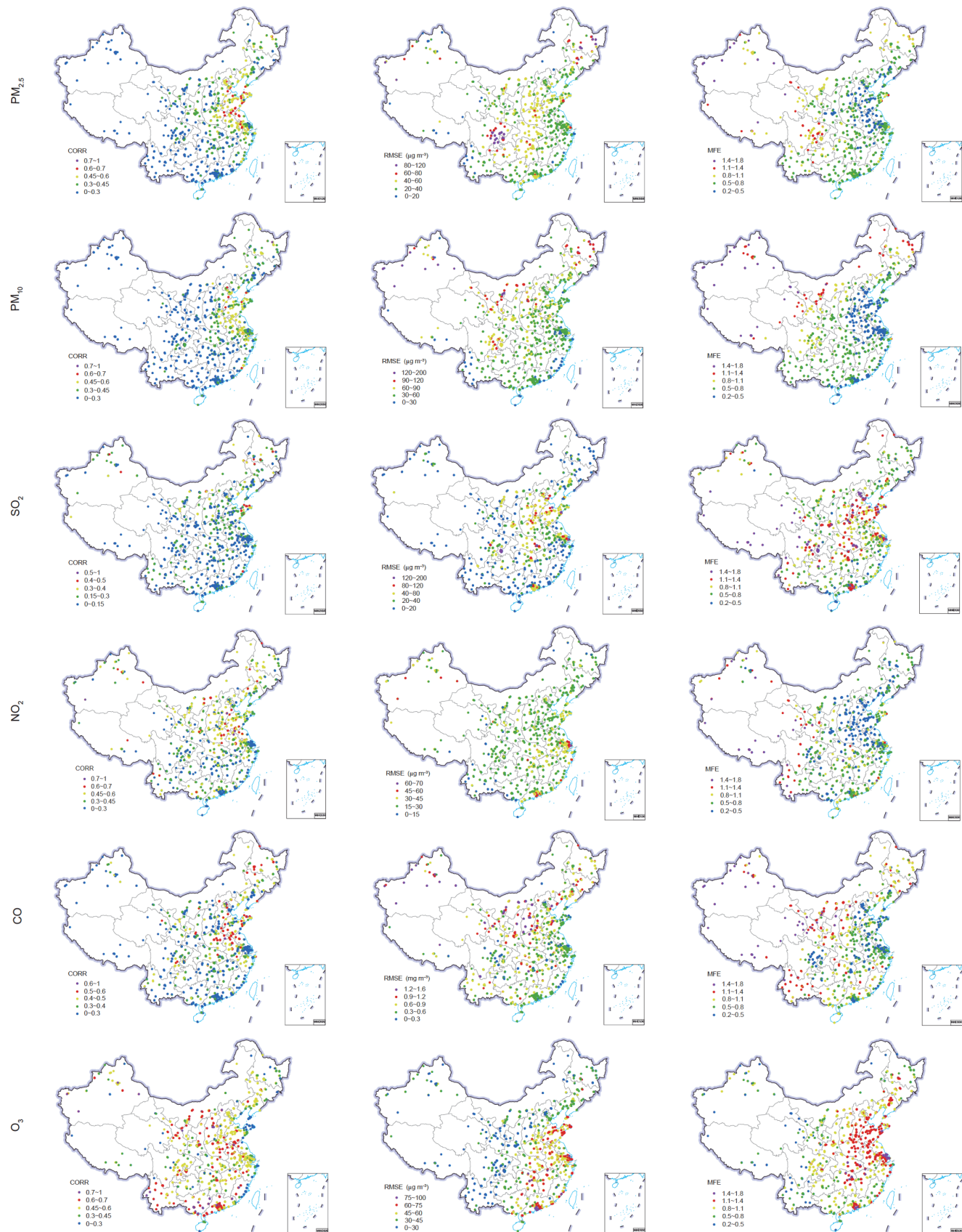


Figure 6 Evaluation indicators CORR, RMSE, and MFE (left-to-right) for the Control experiment at all observation stations for the pollutants $\text{PM}_{2.5}$, PM_{10} , SO_2 , NO_2 , CO , and O_3 (top-to-bottom).

experiment at all observation stations. These indicators differ markedly depending on pollutant. Indeed, in terms of the same pollutants, indicators also vary depending on site and with regard to the different spatial distributions of pollutant concentrations, meteorological conditions, and anthropogenic source emissions. We use MFEs other than RMSEs in this analysis, a different order of magnitude, in order to evaluate the model performance for pollutant forecasting without assimilation. Forecasts of $\text{PM}_{2.5}$, PM_{10} , and NO_2 are superior to those of SO_2 , CO , and O_3 . Thus, in order to analyze assimilation benefits intuitively, differences between Assimilation and Control experiments over the observation sites within a 48 h forecast window for pollutants are presented (Figure 7). The more sites with positive CORR and negative RMSE and MFE differences, the more evident are the improvements by assimilation. The larger the value is, the better the improvement. In terms of both CORR and RMSE differences, DA result in a marked improvement for particulate matter ($\text{PM}_{2.5}$ and PM_{10}) forecasts over China with the exception of just a few regions. At most sites, the CORR of $\text{PM}_{2.5}$ and PM_{10} increased 0–0.1 while RMSE values decreased by $0\text{--}10 \mu\text{g m}^{-3}$, including a marked reduction between 10 and $30 \mu\text{g m}^{-3}$ in the Sichuan Basin where a low center forms. However, the MEF differences show that assimilation did not improve the 48-h forecasts of $\text{PM}_{2.5}$ over the Shandong peninsula, south region of northeast China and east of Jiangsu province. On the contrary, assimilation improves the forecasts of PM_{10} over all these regions and these were particularly significant over western China and over the northern region of northeast China. A number of significant discrepancies are seen between evaluation indicators in the case of SO_2 ; CORR differences show that correlations over north China decreased by 0–0.1, indicating that DA did not improve forecasts for this region. RMSE and MFE differences show that DA significantly improves forecasts over this region; the former decreased by between 5 and $20 \mu\text{g m}^{-3}$ while MFE decreased by 0–0.2, a larger range than seen in other regions. In terms of NO_2 , it is obvious that the CORR of simulations versus observations at more than half of the sites increased by 0–0.1 after assimilation. However, in terms of RMSE and MFE, DA did not improve forecasts over north and east China as well as the Sichuan Basin; evaluation indicators over these areas instead increased due to the adverse influences of other factors, another set of results which demonstrate the positive effects of assimilation on NO_2 forecasts over short timescales, far less than 48 h. RMSE and MFE differences for CO suggest that indicators over other regions were reduced by DA apart from in north and east China and in the Sichuan Basin and a low-value range was also formed across central China where the positive effects of DA were significant and long. There is no evident improvement in correlation but a reduction of 0–0.2 at more than half of the

sites. In terms of O_3 , differences in RMSE remain consistent with those of MFE which indicates that DA has improved O_3 forecasts over China apart from in the southwest and northwest regions. Improvements in south China were higher than in other regions; nevertheless, CORR value differences significantly indicate that the correlation over north China was not improved by DA.

6. Discussion

We have developed a 3DVAR DA system for use with the MOSAIC aerosol assessment mechanism in the WRF-Chem model. The MOSAIC approach employs a size-resolved sectional model for multiple chemical species. We have included a total of 20 control variables including eight aerosol species (encompassing two size-bins in each case) as well as four gaseous pollutants to construct background error covariance matrices. We implemented this 3DVAR system to simultaneously assimilate particulate matter and gaseous pollutant observations.

We performed one-month control and assimilation experiments to evaluate the performance of our 3DVAR system. Comparisons of control forecasts as well as those that encompass assimilation versus observations show that the former system can significantly enhance analyses and the subsequent forecasts of particulate matter and gaseous pollutant mass concentrations. In the first place, vertical structures of background error SD vary amongst distinct aerosol components while background error horizontal and vertical correlations are significantly different among distinct control variables. This relationship is related to differences in the distribution of concentrations of different aerosol species and boundary layer heights. The background error SD of each control variable decreases with height apart for O_3 and encompasses a decline rate that is largest in the upper troposphere. Aerosol species with higher concentrations below 500 m include NO_3i , OINj , NH_4i , SO_4i , OINi , OCi , and ECi , of which OINj reaches the highest concentrations. Concentrations of other components remain much lower. The largest scale change is associated with SO_4i , up to 65.1 km, which indicates that the influence of this pollutant spread farther than other species. In contrast, the smallest correlation length scale is CLj , about one-quarter the scale associated with SO_4i . Indeed, SO_4i spreads over the longest distance while CLj exhibits the shortest spread distance in the vertical, related to concentration. It is also the case that DA significantly improves the initial field of each pollutant. Subsequent to DA, the correlation coefficient of mass concentrations in the analysis field versus observations reached above 0.8, apart from SO_2 (0.60) and CO (0.74) and the root-mean-square error was reduced by more than 50%. Similarly, the mean fraction error was reduced below 0.50 with the

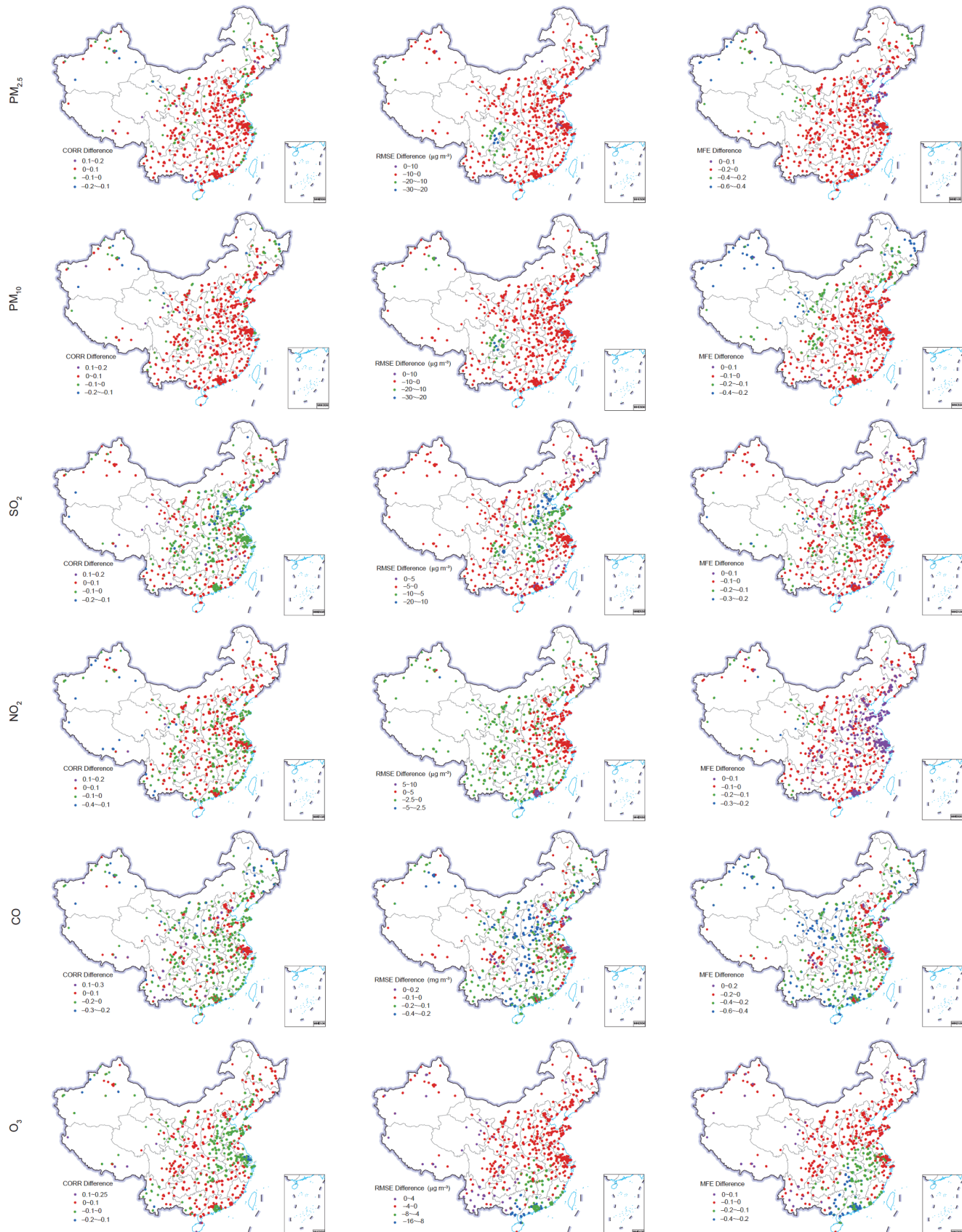


Figure 7 Differences in evaluation indicators CORR, RMSE, and MFE (left-to-right) for the Assimilation minus the Control experiment at all observation stations with respect to the pollutants PM_{2.5}, PM₁₀, SO₂, NO₂, CO, and O₃ (top-to-bottom).

exception of SO_2 (0.51). The positive effects of DA on forecast fields are different depending on pollutants. The DA benefit for $\text{PM}_{2.5}$, PM_{10} , and CO is significant and can last more than 48 h while the benefits for SO_2 and O_3 last up to 8 h. The DA benefit for NO_2 remains relatively poor and only lasts for 3 h and it is also the case that benefits for each pollutant vary in terms of their spatial distribution. The positive effects of DA on $\text{PM}_{2.5}$, PM_{10} , and CO forecasts can last more than 48 h over most regions of China and this process also significantly improves SO_2 forecasts within 48 h over north China. In terms of spatial distribution, however, the DA benefit of NO_2 remains relatively poor compared to other pollutants; sites that exhibit assimilation benefits for this pollutant are sparsely scattered and do not encompass a wide distribution. DA also significantly improves O_3 forecasts within 48 h over China apart from in the southwest and northwest regions while improvements in south China are higher.

The results of this analysis indicate that the positive effects of DA on gaseous pollutant forecast are significant over relatively short times compared with particulate matter, especially for NO_2 . Indeed, compared with $\text{PM}_{2.5}$ and PM_{10} which have relatively long life cycles, chemical species with short life spans such as NO_2 and O_3 experience highly complex and nonlinear photochemical reaction processes over 1 h time scales. The chemical mechanisms of these complex photochemical reactions remain inadequately described (Yang et al., 2015). Considerable uncertainty also remains associated with NO_2 and O_3 forecasts; accuracy largely depends on chemical and physical transport processes. At the same time, analysis of Volatile Organic Compounds (VOC) can also affects NO_2 and O_3 forecasts to some extent. No routine VOC observations are available in China at present and so the assimilation of these is not performed as part of an initial chemical field. This should also be the reason for the short assimilation duration in NO_2 and O_3 forecasts. In species such as SO_2 and CO , the chemical reaction process is relatively long and this means that DA can enhance forecasts to some extent. In the case of species with a long lifespan, a longer forecast range due to DA can be expected than for species with short life spans. Significant differences in pollution level, aerosol compositions, emissions, and meteorological conditions over each region will lead to distinct assimilation benefits.

In order to continuously improve the accuracy of forecasts, the cycle assimilation method should be adopted to repeatedly introduce observation information into models. This means that observations and background values can be fully integrated to generate an enhanced initial field for simulations, leading to improved and longer assimilation benefits.

Acknowledgements

We are grateful to the National Centers for

Environmental Prediction for providing the FNL Operational Global Analysis data as well as to the China National Environmental Monitoring Centre for making observational pollutant data available. This work was supported by the National Key R&D Program of China (Grant No. 2017YFC0209803) and the National Natural Science Foundation of China (Grant Nos. 41775123 & 41805092).

References

- Benedetti A, Fisher M. 2007. Background error statistics for aerosols. *QJR Meteorol Soc*, 133: 391–405
- Binkowski F S, Roselle S J. 2003. Models-3 Community Multiscale Air Quality (CMAQ) model aerosol component 1. Model description. *J Geophys Res*, 108: 4183
- Bouttier F, Courtier P. 2002. Data assimilation concepts and methods March 1999. Meteorological Training Course Lectures Series. ECMWF, 776: 59
- Boylan J W, Russell A G. 2006. PM and light extinction model performance metrics, goals, and criteria for three-dimensional air quality models. *Atmos Environ*, 40: 4946–4959
- Chen D, Liu Z, Fast J, Ban J. 2016. Simulations of sulfate–nitrate–ammonium (SNA) aerosols during the extreme haze events over northern China in October 2014. *Atmos Chem Phys*, 16: 10707–10724
- Cheng X, Liu Y, Xu X, You W, Zang Z, Gao L, Chen Y, Su D, Yan P. 2019. Lidar data assimilation method based on CRTM and WRF-Chem models and its application in $\text{PM}_{2.5}$ forecasts in Beijing. *Sci Total Environ*, 682: 541–552
- Cui Y, Wang Z, Zhu J, Fu Q. 2006. A preliminary study on data assimilation for numerical air quality model prediction (in Chinese). *Climat Environm Res*, 11: 616–626
- Derber J, Bouttier F. 1999. A reformulation of the background error covariance in the ECMWF global data assimilation system. *Tellus A*, 51: 195–221
- Eibner H, Schmidt H. 1999. A four-dimensional variational chemistry data assimilation scheme for Eulerian chemistry transport modeling. *J Geophys Res*, 104: 18583–18598
- Elbern H, Schmidt H, Ebel A. 1997. Variational data assimilation for tropospheric chemistry modeling. *J Geophys Res*, 102: 15967–15985
- Elbern H, Schmidt H. 2001. Ozone episode analysis by four-dimensional variational chemistry data assimilation. *J Geophys Res*, 106: 3569–3590
- Errera Q, Daerden F, Chabirillat S, Lambert J C, Lahoz W A, Viscardi S, Bonjean S, Fonteyn D. 2008. 4D-Var assimilation of MIPAS chemical observations: Ozone and nitrogen dioxide analyses. *Atmos Chem Phys*, 8: 6169–6187
- Feng S, Jiang F, Jiang Z, Wang H, Cai Z, Zhang L. 2018. Impact of 3DVAR assimilation of surface $\text{PM}_{2.5}$ observations on $\text{PM}_{2.5}$ forecasts over China during wintertime. *Atmos Environ*, 187: 34–49
- Gao M, Guttikunda S K, Carmichael G R, Wang Y, Liu Z, Stanier C O, Saide P E, Yu M. 2015. Health impacts and economic losses assessment of the 2013 severe haze event in Beijing area. *Sci Total Environ*, 511: 553–561
- Grell G A, Peckham S E, Schmitz R, McKeen S A, Frost G, Skamarock W C, Eder B. 2005. Fully coupled “online” chemistry within the WRF model. *Atmos Environ*, 39: 6957–6975
- Han S, Feng Y, Bian H, Tie X, Xie Y, Li X, Sun M. 2008. Numerical simulation of diurnal variation of major pollutants with WRF-Chem model in Tianjin (in Chinese). *China Environm Sci*, 28: 828–832
- Jiang Z, Liu Z, Wang T, Schwartz C S, Lin H C, Jiang F. 2013. Probing into the impact of 3DVAR assimilation of surface PM_{10} observations over China using process analysis. *J Geophys Res Atmos*, 118: 6738–6749
- Jin L, Zang Z, Pan X, Wang T, Hao Z, Jiang Z. 2006. Data assimilation and application experiments of $\text{PM}_{2.5}$ and $\text{PM}_{2.5-10}$ during Nanjing Youth Olympic Games (in Chinese). *China Environm Sci*, 36: 331–341
- Liu Z, Liu Q, Lin H C, Schwartz C S, Lee Y H, Wang T. 2011. Three-dimensional variational assimilation of MODIS aerosol optical depth:

- Implementation and application to a dust storm over East Asia. *J Geophys Res*, 116: D23206
- Lin C, Wang Z, Zhu J. 2008. An Ensemble Kalman Filter for severe dust storm data assimilation over China. *Atmos Chem Phys*, 8: 2975–2983
- Li Z, Zang Z, Li Q B, Chao Y, Chen D, Ye Z, Liu Y, Liou K N. 2013. A three-dimensional variational data assimilation system for multiple aerosol species with WRF/Chem and an application to PM_{2.5} prediction. *Atmos Chem Phys*, 13: 4265–4278
- Ma M, Yang X, Ding F, Tan Z, Li X. 2018. Temporal and spatial distribution of atmospheric pollutants between northern China and southern China (in Chinese). *Environ Sci Technol*, 41: 187–197
- Niu T, Gong S L, Zhu G F, Liu H L, Hu X Q, Zhou C H, Wang Y Q. 2007. Data assimilation of dust aerosol observations for CUACE/Dust forecasting system. *Atmos Chem Phys Discuss*, 7: 8309–8332
- Parrish D F, Derber J C. 1992. The National Meteorological Center's spectral statistical-interpolation analysis system. *Mon Wea Rev*, 120: 1747–1763
- Pagowski M, Grell G A. 2012. Experiments with the assimilation of fine aerosols using an ensemble Kalman filter. *J Geophys Res*, 117: D21302
- Pagowski M, Grell G A, McKeen S A, Peckham S E, Devenyi D. 2010. Three-dimensional variational data assimilation of ozone and fine particulate matter observations: Some results using the Weather Research and Forecasting-Chemistry model and Grid-point Statistical Interpolation. *Q J R Meteorol Soc*, 136: 2013–2024
- Shang K, Shang Z, Jia X, Zhou K, Du H. 2018. Characteristic analysis of air pollutant concentration on representative stations in Chinese mainland (in Chinese). The 35th Annual Meeting of Chinese Meteorological Society, S13, Atmospheric Physics and Atmospheric Environment. 191–204
- Saide P E, Kim J, Song C H, Choi M, Cheng Y, Carmichael G R. 2014. Assimilation of next generation geostationary aerosol optical depth retrievals to improve air quality simulations. *Geophys Res Lett*, 41: 9188–9196
- Schwartz C S, Liu Z, Lin H C, McKeen S A. 2012. Simultaneous three-dimensional variational assimilation of surface fine particulate matter and MODIS aerosol optical depth. *J Geophys Res*, 117: D13202
- Song H, Wang K, Zhang Y, Hong C, Zhou S. 2017. Simulation and evaluation of dust emissions with WRF-Chem (v3.7.1) and its relationship to the changing climate over East Asia from 1980 to 2015. *Atmos Environ*, 167: 511–522
- Tang Y, Pagowski M, Chai T, Pan L, Lee P, Baker B, Kumar R, Delle Monache L, Tong D, Kim H C. 2017. A case study of aerosol data assimilation with the Community Multi-scale Air Quality Model over the contiguous United States using 3D-Var and optimal interpolation methods. *Geosci Model Dev*, 10: 4743–4758
- Tombette M, Mallet V, Sportisse B. 2009. PM₁₀ data assimilation over Europe with the optimal interpolation method. *Atmos Chem Phys*, 9: 57–70
- Xue W, Wang J, Yang J, Lei Y, Wang Y, Chen X. 2013. Domestic and foreign research progress of air quality model (in Chinese). *Environ Sust Developm*, 38: 14–20
- Yang Y R, Liu X G, Qu Y, An J L, Jiang R, Zhang Y H, Sun Y L, Wu Z J, Zhang F, Xu W Q, Ma Q X. 2015. Characteristics and formation mechanism of continuous hazes in China: A case study during the autumn of 2014 in the North China Plain. *Atmos Chem Phys*, 15: 8165–8178
- Zaveri R A, Easter R C, Fast J D, Peters L K. 2008. Model for simulating aerosol interactions and chemistry (MOSAIC). *J Geophys Res*, 113: D13204
- Zhang R H, Li Q, Zhang R N. 2014. Meteorological conditions for the persistent severe fog and haze event over eastern China in January 2013. *Sci China Earth Sci*, 57: 26–35
- Zhao Z, Wei Y, Zhang X, Qin W, Xie H. 2015. The correlation analysis of Nanjing haze days and meteorological factors (in Chinese). *China Environ Sci*, 35: 3570–3580

(Responsible editor: Tijian WANG)